Nanoparticles Formed in Picosecond Laser Argon Crystal Interaction

Xinwei Wang
e-mail: xwang3@unl.edu
Department of Mechanical Engineering,
N104 Walter Scott Engineering Center,
The University of Nebraska-Lincoln,
Lincoln, NE 68588-0656

Xianfan Xu
School of Mechanical Engineering,
Purdue University,
West Lafayette, IN 47907-1288

In this work, Molecular Dynamics simulations are conducted to attain thermal and mechanical characteristics of nanoparticles formed in laser materials interaction. It reveals that nanoparticles originate from intense vapor phase explosion. A gas-like structure is observed in nanoparticles in the initial stage of formation. After a short time of evolution, a typical liquid structure is revealed in particles. As a direct consequence of atoms escaping from the particle surface, the temperature of nanoparticles reduces to an undercooling point from the initial super-heating state. Furthermore, it indicates that movements of nanoparticles are dominated by those normal to the target surface.
[DOI: 10.1115/1.1621898]

Keywords: Heat Transfer, Laser, Molecular Dynamics, Nanoscale, Thermophysical

Introduction

In recent years, it has become more tempting to attach significant research interest to nanoparticles formed in short pulsed laser materials interaction due to their strong impact on micro/nanoscale manufacturing and thin film deposition. Ultrafast pulsed laser heating and the extremely small particle size impose considerable difficulty on experimental studies of the underlying physical origins as well as the in-situ thermal and mechanical characteristics associated with nanoparticles.

Interaction of the ultrafast laser pulse with the target material and the resulting material ablation are endowed with strong nonlinear, coupled optical, thermal, and mechanical processes that significantly complicate theoretical analysis. Molecular Dynamics (MD) simulation, which studies physical processes at the molecular/atomic level, is capable of providing systematic and integrated information of laser heating, material evaporation and nanoparticle formation.

A number of MD simulations have been reported on studying laser interaction with various targets. For semi-conductor materials, Kluge et al. [1] studied picosecond (ps) laser heating of a small silicon target comprising 216 atoms. Recently, ultrashort pulsed laser interaction with a larger silicon target constituted of 23,000 atoms was investigated by Herrmann et al. [2]. Laser-induced ultrafast phase transition in carbon was explored by Jeschke et al. [3] for a target of 216 atoms. As for laser metal interaction, laser heating of a metal surface was considered by Häkkinen and Landman [4] with taking into account the two-step heat transfer [5], and by Ohmura and Fukumoto [6]. Interaction of ultrafast laser with dielectrics and organic materials has been addressed by Kotake and Kuroki [7] and Zhigilei et al. [8], respectively. The quantum-mechanical effects in ultrashort laser materials interaction have been explored by Shibahara and Kotake [9] and Silverstrelli and Parrinello [10]. More recently, substantial details about the thermal and thermomechanical phenomena in ps laser interaction with large targets were reported by Etcheverry and Mesaros [11] and Wang and Xu [12,13]. Despite the large number of MD work pertinent to laser materials interaction, few MD simulations investigated nanoparticles formed in pulsed laser materials interaction [14–16]. Considerable details pertaining to the ablation process from which clusters originate have been reported by Zhigilei et al. [15] on the basis of the MD simulation of ps laser organic solid interaction. It was pointed out by Ohmura et al. [16] that nanoparticles formed in ps laser metal interaction ejected from the target surface at a speed of several thousands of meters per second. To date, knowledge of formation and evolution of nanoparticles, as well as their in-situ thermal and mechanical properties are still lacking, thereby placing impediments on further understanding and optimizing pulsed laser materials processing.

In this work, MD simulations are carried out to investigate ps laser material interaction. Emphasis is placed on formation and evolution of nanoparticles during and after laser heating. Moreover, thermal and mechanical characteristics of nanoparticles, such as structure, temperature, and velocities are addressed in considerable detail. In this paper, methodologies employed in the MD simulation are outlined first, and then MD simulation results are presented to address various thermal and mechanical issues associated with nanoparticles.

Methodologies of the MD simulation

The problem to be studied in this work is associated with an argon crystal at an initial temperature of 50 K subjected to ps pulsed laser heating. The basic problem involves solving the Newtonian equations for each atom interacting with its neighbors,

$$m_i \frac{d^2 r_i}{dt^2} = \sum F_{ij} \tag{1}$$

where m_i and r_i are the mass and position of atom i, respectively, and m_i is taken as 6.63×10^{-26} kg for argon. F_{ij} stands for the interaction force between atoms i and j, and is computed from the Lennard-Jones (LJ) potential as $F_{ij}=-\partial\phi_{ij}/\partial r_{ij}$ with $r_{ij}=r_i-r_j$. The Lennard-Jones potential ϕ_{ij} is of the form

$$\phi_{ij}=4\varepsilon\left[\left(\frac{\sigma_e}{r_{ij}}\right)^{12}-\left(\frac{\sigma_e}{r_{ij}}\right)^{6}\right] \tag{2}$$

where ε is the LJ well depth parameter, and the corresponding value for argon is 1.653×10^{-21} J. σ_e is referred to as the equilibrium separation parameter, and is 0.3406 nm for argon [12].

A time step of 25 fs is applied in the simulation [11]. The interaction between particles is neglected when their distance exceeds a particular length r_c, namely, the cutoff distance. For ar-

Contributed by the Heat Transfer Division for publication in the JOURNAL OF HEAT TRANSFER. Manuscript received by the Heat Transfer Division October 25, 2002; revision received July 7, 2003. Associate Editor: V. P. Carey.

gon, the widely accepted value of $2.5\sigma_e$ for r_c is applied in this work [12]. Details of the computation are published elsewhere [12,17].

Laser beam absorption in the target is achieved by exciting the kinetic energy of atoms, which is fulfilled by scaling the velocities of atoms with an appropriate factor. This factor is calculated as

$$\chi=\left[1+\frac{\Delta E}{\frac{1}{2}\sum_{i=1}^{N} m_i\cdot[(v_{i,1}-\overline{v_1})^2+(v_{i,2}-\overline{v_2})^2+(v_{i,3}-\overline{v_3})^2]}\right]^{1/2} \tag{3}$$

where $v_{i,j}$ and $\overline{v_j}$ $(j=1,2,3)$ are velocities of atom i and the average velocity in the x, y, and z directions for atoms in a layer normal to the laser beam. ΔE is the laser beam energy deposited in the layer during one time step, and N is the number of atoms within the layer. The new velocity $v'_{i,j}$ of atom i is calculated as

$$v'_{i,j}=(v_{i,j}-\overline{v_j})\cdot\chi+\overline{v_j} \qquad j=1,2,3 \tag{4}$$

This laser energy absorption model de-emphasizes the details of laser materials interaction, for which the quantum-mechanical effect needs to be accounted for, but is not predominant. The characteristic time of laser material interaction (<1 ps) is much smaller than the time associated with the laser pulse in this work. Hence nanoparticle formation and the thermal and mechanical information associated with them can still be investigated using the current absorption model in the absence of detailed knowledge of laser materials interaction. Exponential laser beam absorption is presumed in the computation with an absorption depth of τ. In this work, in lieu of recovering a specific experimental condition, the value of τ is chosen to reflect the fact of volumetric absorption of the laser beam. The presumed value (2.5 nm) of τ indicates that the laser beam will be absorbed within a distance of about 10 nm from the target surface. Therefore, the back side of the target will not see the direct effect of laser beam absorption. The laser pulse assumes a temporal Gaussian distribution with a FWHM (full width at half maximum) of 5 ps centered at 10 ps.

The MD computational domain is constructed in a fashion to embody extra spaces above and below the target, allowing macromotion of atoms in the z direction. Periodic boundary conditions are applied at the boundaries in the x and y directions, and free boundary conditions at the boundaries in the z direction. The target is initially constructed based upon the fcc (face-centered cubic) lattice structure of a lattice constant 0.5414 nm [12] with the (100) surface facing the laser beam. Initial velocities of atoms are specified randomly from a Gaussian distribution based on the expected temperature of 50 K. Before laser heating starts, the sample is thermalized for 100 ps to reach thermal equilibrium [11,12].

Results and Discussion

In the results that follow, a freestanding film of 90 fcc unit cells (48.73 nm) in the x and y directions, and 60 fcc unit cells (32.48 nm) in the z direction is irradiated with a single laser pulse of 1.2 J/m^2. This laser energy was proved high enough to induce phase explosion and formation of nanoparticles for argon crystal [12]. The thickness of the sample (32.48 nm) is much larger than the penetration depth of the laser beam ($\sim$10 nm), which ensures complete absorption of the laser beam. The computational domain measures 48.726 nm in the x and y directions, and 553.94 nm in the z direction with the back side of the film located at 8.55 nm. Schematic of the computational domain is shown in Fig. 1. A total of 1,944,000 atoms are tracked in the simulation. Parallel computation was conducted on a two-processor Xeon workstation using OpenMP (Open Multiple Processing).

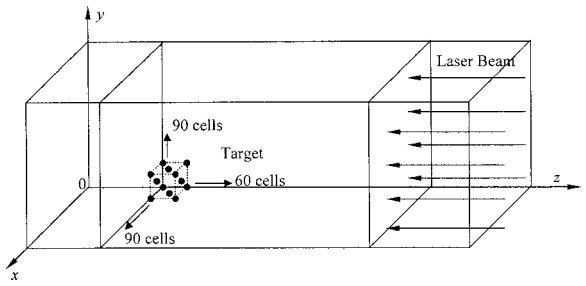

Fig. 1 Schematic of the computational domain

Formation of Nanoparticles. The manner in which nanoparticles are formed in ps laser argon interaction is delineated in Fig. 2, which presents snap shots of atomic positions at different moments. For the purpose of illustration, only the domain of $0\leqslant x\leqslant 20$ nm, $0\leqslant y\leqslant 20$ nm, and $30\leqslant z\leqslant 90$ nm is illustrated. It is important to note that when the laser pulse stops ($t=15$ ps), thermal expansion is predominant and intense movements of atoms are observed at the target surface. Between 20 and 40 ps, phase explosion is taking place and becoming more intense with time. At 40 ps, it is evident that the thermal expansion of the material is replaced by an intense phase explosion indicated by the strong non-uniform atomic distribution in space. Plots at 60 ps through 150 ps are characterized by large clusters separating from each other to form individual particles. As a direct consequence of the surface tension force, the initial irregular nanoparticles gradually change to spheres. This process is demonstrated in plots of 200 ps through 500 ps.

The detailed formation process of a particular particle is delineated in Fig. 3. For the purpose of citation, this particle is termed particle β in the following sections. Since Fig. 2 only displays part of the computational domain, particle β can not be identified in Fig. 2. It is much pronounced in Fig. 3 that the particle starts with an irregular shape (70 ps) and concludes with a spherical one (500 ps). Before 70 ps, this particle does not separate from the target and can not be well defined. The initial irregular shape originates from the non-uniform phase explosion, and it takes quite a long time ($\sim$400 ps) for the particle to become a sphere. From 125 ps to 300 ps, the nanoparticle experiences an oscillation process, which diminishes gradually due to the presence of the inherent retarding force. The particle formation is also characterized by a shrinking process indicated by the presence of the initial loose atom distribution in space and the final much more dense distribution.

Figure 4(a) presents the variation of the particle number versus time, while Fig. 4(b) details the onset of particle formation. In Fig. 4, particle sizes are roughly sorted into several groups based on the number of atoms in a particle. This rough classification can readily reveal the trend of the formation of particles during laser-material interaction. Detailed particle size distribution was discussed elsewhere [18]. To define a particle, two atoms are treated as within the same particle if their distance does not exceed 0.40 nm, which is the nearest neighbor distance of argon atoms at the boiling point. It is found that particles defined by this criterion precisely represent the particles observed in the snap shot of atomic positions (Fig. 2). In Fig. 4 it is apparent that single atoms start coming out substantially at 10 ps through 30 ps, and stabilize at a number of about 50,000 after 200 ps. For dimers and particles comprising $3\sim100$ atoms, their populations quickly reach a peak value at about 25 ps, and decay over a quite long time of about 300 ps. The reduction of the particle number is a consequence of losing atoms from the particle surface or smaller particles combining to form a bigger one. Particles consisting of 101 $\sim$1000 atoms are characterized with an emergence time delay of 10 ps in comparison with smaller particles and single atoms. In

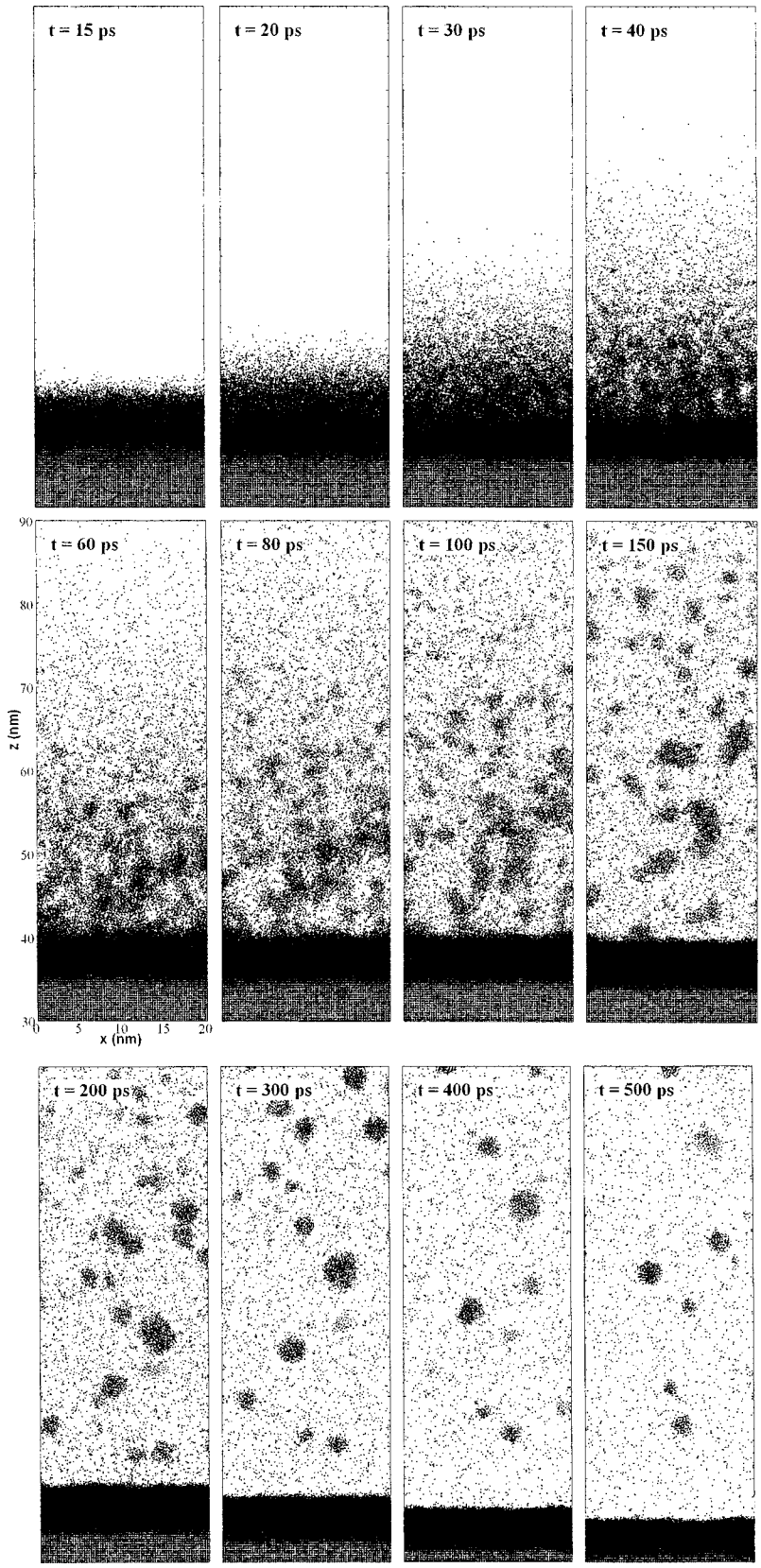

Fig. 2 Snap shots of atomic positions at different moments

other words, particles composed of 100 atoms or less start emerging during laser heating (10 ps), while particles comprising 101 atoms or more start appearing after laser heating (20 ps).

Escape of atoms from the particle surface could reduce the size of the particle substantially, and this effect is delineated in Fig. 5, which presents the temporal variation of the diameter of particle

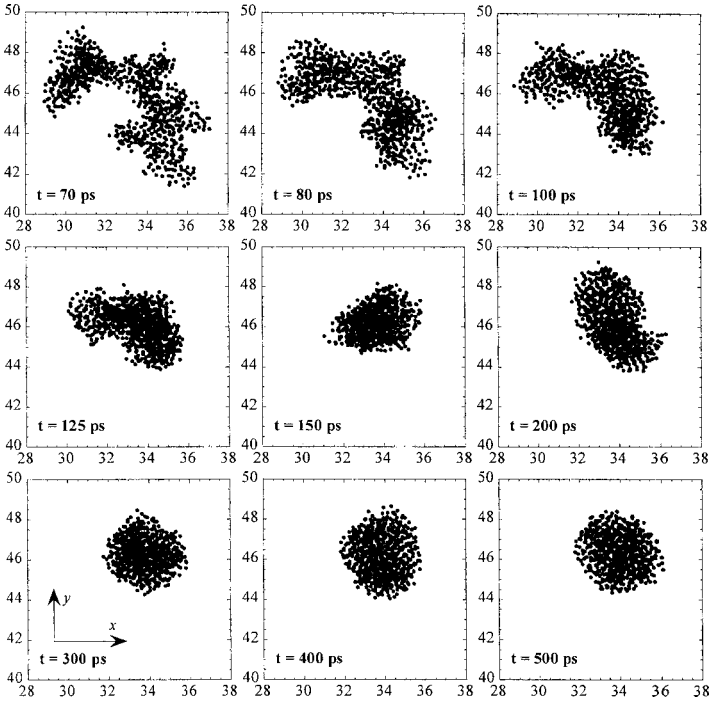

Fig. 3 Detailed formation process of particle β. The unit of the coordinates is nm.

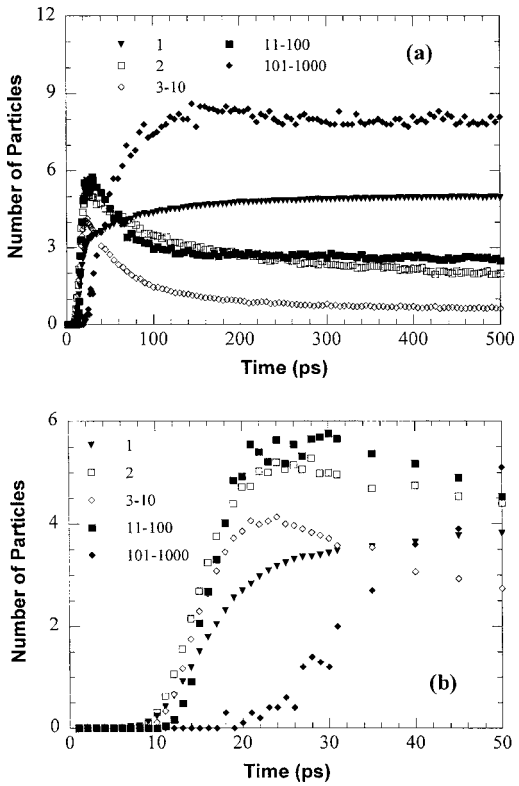

Fig. 4 Variation of the particle number versus time. Units of particle numbers are: 10^4 for monomers, 10^3 for dimers and particles consisting of 3 to 10 atoms, 10^2 for particles consisting of 11–100 atoms, and 10 for particles consisting of 101–1000 atoms.

β. The diameter of the nanoparticle is an effective value corresponding to a sphere comprising the same number of atoms at a fixed density that is evaluated at 500 ps. The sudden and temporary drop of the diameter at 110 ps is attributed to a temporary separation of a cluster from the particle. When this cluster separates from the particle, it is not accounted for when defining the particle volume, thereby inducing a temporary reduction in the particle diameter. It is seen in Fig. 5 that after 500 ps the diameter of the particle decreases by 7%, meaning a volume reduction of about 20%.

Structure of Nanoparticles. It is a common practice to work with the radial distribution function when studying material structure. In general, the radial distribution function is defined as the ratio of the number of atoms at a distance r from a given atom compared with the number of atoms at the same distance in the ideal gas with the same density. In lieu of using the time-varying density of the particle as the reference, a constant reference density is used which is evaluated at 500 ps. The manner in which the

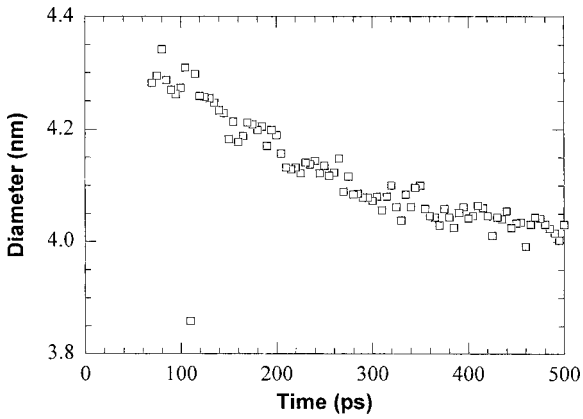

Fig. 5 Temporal variation of the diameter of particle β

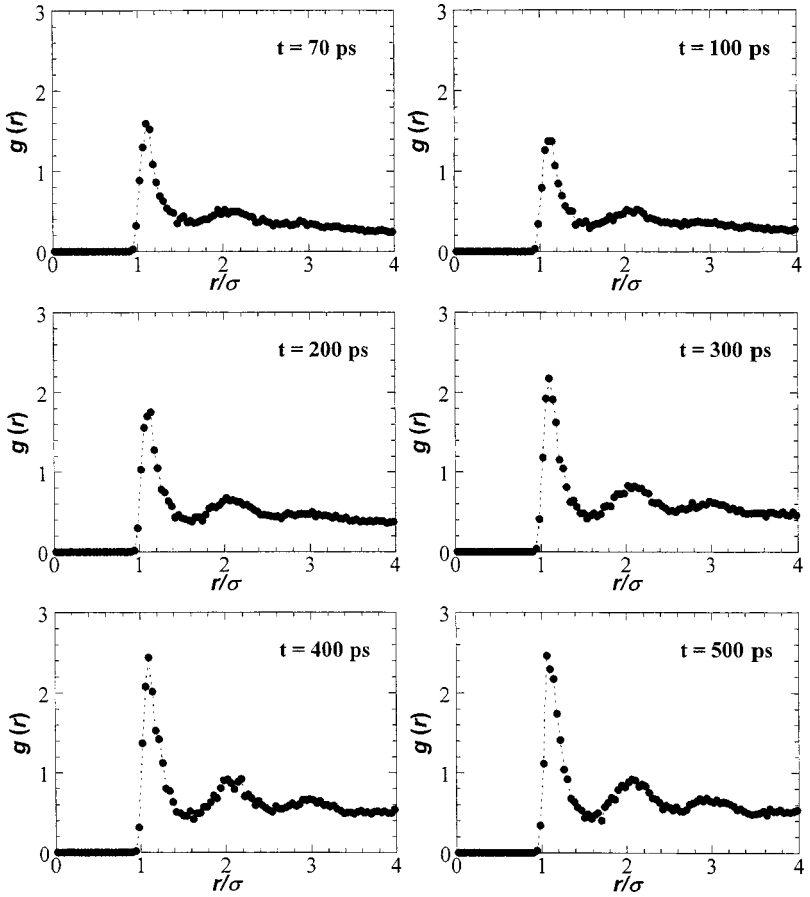

Fig. 6 Radial distribution function within particle β at different times

radial distribution function is modified makes it possible to acquire knowledge of the material density by looking into the absolute value of the radial distribution function while its shape reflects the material structure.

The radial distribution function $g(r)$ for particle β is plotted in Fig. 6. It is observed that the evolution of the radial distribution function is characterized with two features. One feature is that the structure of the particle undergoes a transition from the initial gas-like structure to the final typical liquid structure. At 70 ps, it is pronounced that only the short-range order is preserved, and the long-range order is insignificant as indicated by the presence of the second weak peak. This gas-like structure remains until 300 ps while the second peak is becoming more prominent. At 300 ps, a weak third peak emerges, indicating that the liquid structure is becoming significant. After another 200 ps transition, the liquid structure is predominant, which is dictated by the three strong peaks in the radial distribution function at 500 ps.

The other feature characterizing the structural variation is the continuous condensation of atoms in space. The absolute value of the radial distribution function provides a measure of the amount by which the number density of atoms is evaluated. It is evident in Fig. 6 that besides the shape transition of the radial distribution function, its absolute value increases over the 500 ps period. In particular, the first peak has a maximum value of 1.6 at 70 ps, and this number increases to 2.6 at 500 ps. For $g(r)$ of $r/\sigma=4.0$, its value increases substantially from 0.25 at 70 ps to 0.54 at 500 ps. The increase of the radial distribution function suggests that at a distance r from a given atom, more atoms can be found, meaning atoms are getting closer to each other. Based on the absolute value of the radial distribution function, the number density of atoms of particle β almost doubles to a first approximation.

Based on the definition of the radial distribution function used in this work, the average density (n) of the particle is related to $g(r)$ as

$$n \propto \int_0^{r_{\max}} g(r) r^2 dr \tag{5}$$

Figure 7 presents the density of particle β calculated using Eq. (5). In Fig. 7, it is evident that the density increases with time. The density at 500 ps is 12.78, which is 1.78 times the density at 70 ps (7.19), confirming the approximation conducted above. Both losing atoms from the particle surface and the decrease in intermo-

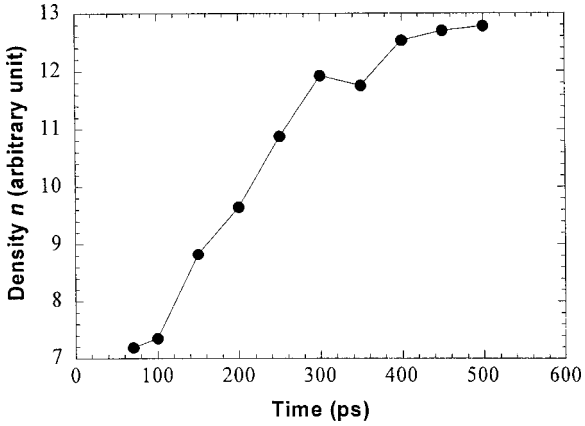

Fig. 7 Density of particle β at different times

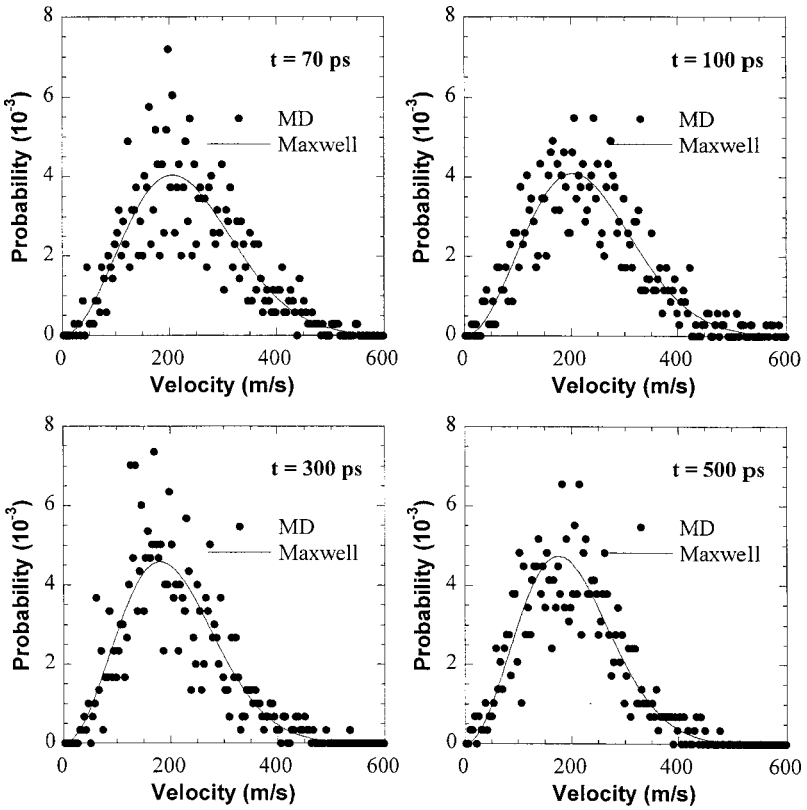

Fig. 8 Velocity distribution in comparison with the Maxwellian distribution within particle β

lecular spacing could reduce the size of the particle. As seen in Fig. 7, the decrease of intermolecular spacing can reduce the volume of the particle by about 44%. As discussed above (Fig. 5), escape of molecules from the particle surface reduces the volume of particle β by about 20% (Fig. 5), which is smaller than, but comparable to, the effect of decrease of intermolecular spacing.

Temperature of Nanoparticles. It is important to be cognizant of the thermal equilibrium status of nanoparticles when exploring their temperature variation. The thermal equilibrium status is examined by comparing the atom velocity distribution with the Maxwellian distribution. Figure 8 shows the comparison of the velocity distribution of atoms within particle β. It is evident that at all times the velocity distribution follows the Maxwellian distribution well yet with noticeable deviations attributed to the small number of atoms within the particle.

The temperature of the particle is calculated using

$$\frac{3}{2}Nk_BT=\sum_{i=1}^{N} m_i\frac{1}{2}(v_{i,1}^2+v_{i,2}^2+v_{i,3}^2) \tag{4}$$

where N is the number of atoms within the particle, k_B is the Boltzmann's constant (1.38×10^{-23} J/mol·K), and $v_{i,j}$ ($j=1,2,3$) is the velocity of atom i in the x, y, and z directions.

Temporal variation of the temperature of particle β is plotted in Fig. 9. It is prominent that the temperature decays with time. Atoms escaping from the particle surface take away a considerable amount of energy. As a result, the particle temperature experiences a decaying process as illustrated in Fig. 9. At 70 ps, the particle is at a temperature above 100 K, which exceeds the boiling point (87.3 K) of argon, indicating the existence of superheating. On the other hand, the particle temperature reduces to as low as 75 K at 500 ps, much lower than the melting point of argon (83.8 K) while the particle is still at the liquid state as described before. Hence under-cooling occurs for particles formed in ps laser materials interaction. This phenomenon is attributed to the rapid cooling induced by escape of atoms from the particle surface while the particle itself does not have enough time to solidify.

The temperature variation described in the preceding paragraph exists for all particles comprising a large number of atoms for which the temperature concept is still valid. Figure 10 presents the temperature distribution versus the particle size at different times. For particles of less than 2 nm in diameter, their temperature cannot be defined in the strict physical sense since thermal equilibrium can not establish due to the small number of atoms within the particle. Hence Fig. 10 only plots the temperature of particles with a diameter of 2 nm or greater. It is evident that at 500 ps all

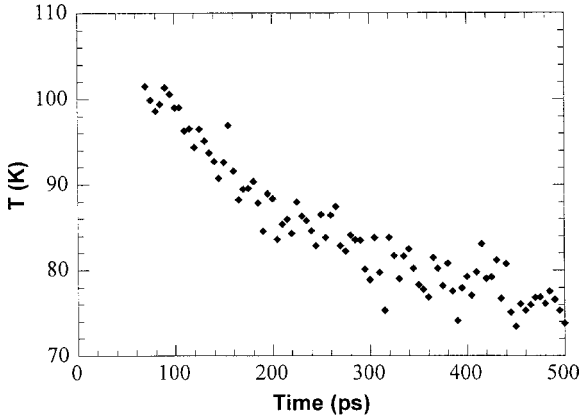

Fig. 9 Temperature of particle β at different times

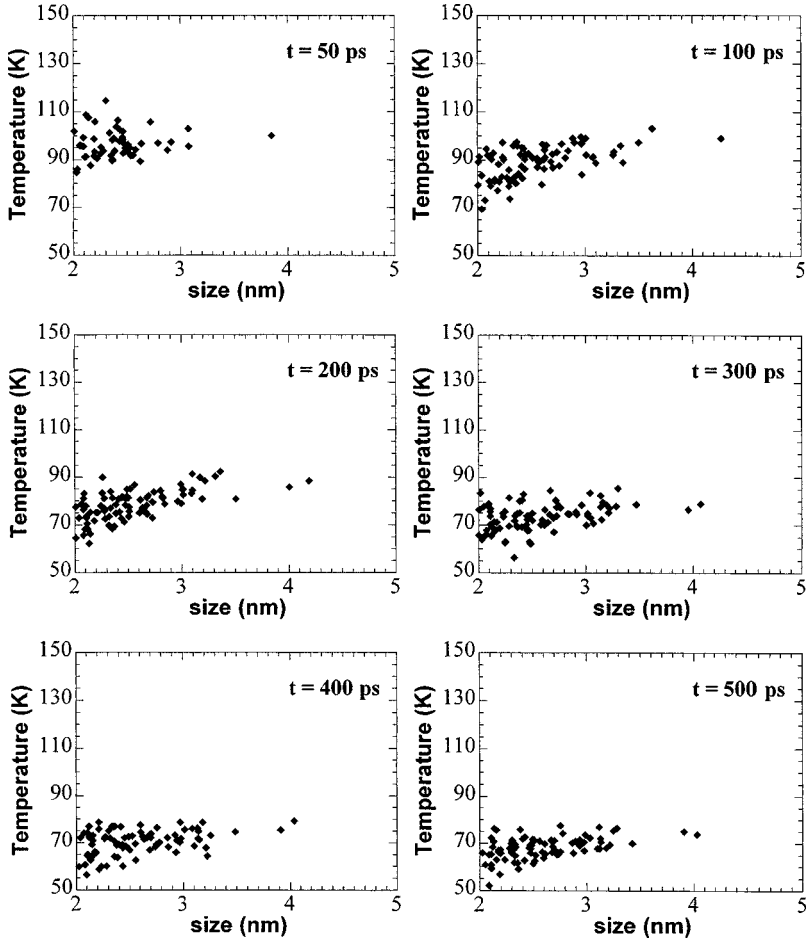

Fig. 10 Temperature distribution versus the particle size at different times

particles are at temperatures below the melting point of argon even though their initial temperatures (50 ps) are above the boiling point.

Velocities of Nanoparticles. The temporal variation of velocities of particle β is presented in Fig. 11. It is much noticeable in Fig. 11 that velocities in the x and y directions are one order of magnitude smaller than that in the z direction. Therefore, movements of the particle are dominated by those in the z direction. It is observed that initially the particle has a relatively high velocity in the x and y directions ($\sim$8 m/s) and conclude with a much smaller velocity of about 3 m/s. For the movement in the z direction, the particle starts with a velocity of about 130 m/s and picks up speed to a higher level of about 143 m/s at 500 ps. The velocities presented in Fig. 11 shows oscillation with time, which is attributed to escape of atoms from the particle surface. When an atom escapes from the particle, the momentum (velocity) of the particle changes accordingly due to momentum conservation. Since atoms escaping from the particle surface have different momentum, velocities of the particle show some up-and-down behavior with time.

Velocities of particles versus the diameter are shown in Fig. 12. It is apparent that the maximum velocity of smaller particles exceeds that of larger ones. For larger particles, their velocity is only about tens of meters per second or less in the x and y directions, while the maximum velocity in the z direction is about 100 m/s or less. This demonstrates that the z direction movement is predominant for nanoparticles formed in ps laser materials interaction. Another noticeable characteristic of the particle movement is that particles move with the same probability in the opposite x and y directions. In contrast, for movement in the z direction, the velocity in the negative z direction is observed for smaller particles, but is insignificant in comparison with that in the positive z direction. For larger particles, only few move slowly in the negative z direction while most of them move in the positive z direction.

Conclusion

In this work, MD simulations were carried out to study nanoparticles formed in ps laser materials interaction. Substantial details of nanoparticle formation as well as their thermal and mechanical characteristics were uncovered. It was revealed that nanoparticles originated from an intense vapor phase explosion process. Small particles started coming out during laser heating while larger ones emerged after laser heating. Nanoparticles started with a gas-like structure of a super-heating state and concluded with a typical liquid structure at an under-cooling state. The temperature reduction of nanoparticles was attributed to atoms escaping from the particle surface. Moreover, nanoparticles underwent a substantial volume reduction due to the atomic escape from the particle surface and a decrease of intermolecular spacing. Movements of nanoparticles were dominated by those in the z direction. In the x and y directions, nanoparticles have the same probability of moving in opposite directions, while in the z direction, the movement in the positive direction is predominant.

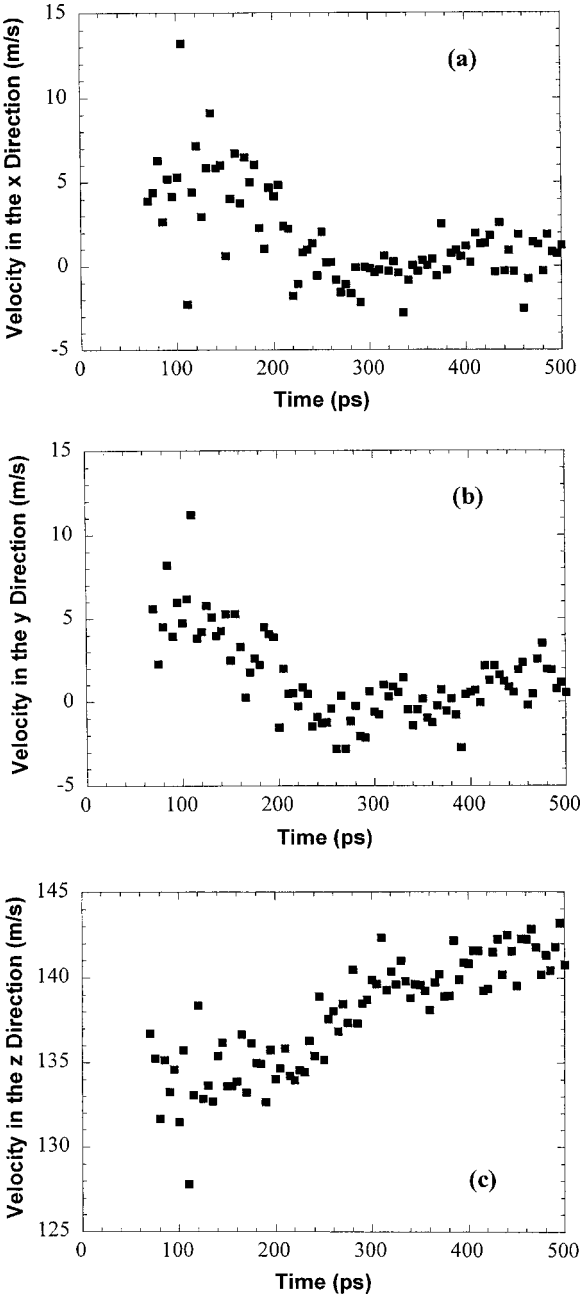

Fig. 11 Temporal variation of velocities of particle β

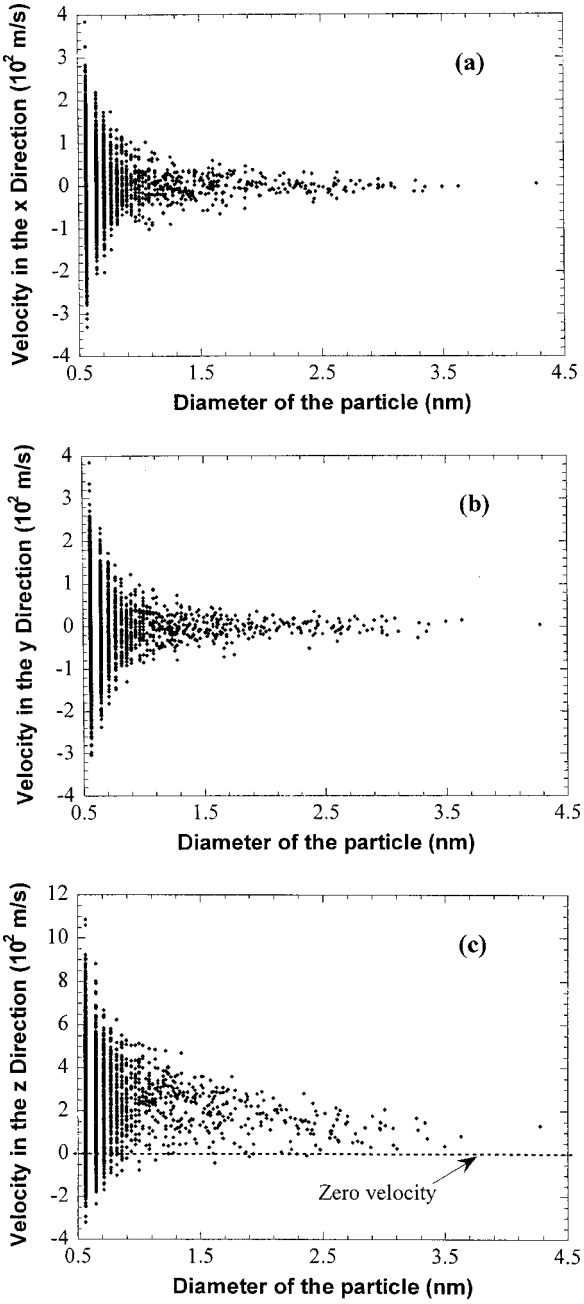

Fig. 12 Velocity distribution versus the diameter of particles at 100 ps

Acknowledgment

One of the authors (X. Wang) is thankful for the financial support of the start-up fund from the College of Engineering and Technology and the Department of Mechanical Engineering at the University of Nebraska - Lincoln. The authors also thank the helpful discussion with Dr. David A. Willis of the Department of Mechanical Engineering at the Southern Methodist University.

Nomenclature

ΔE = the laser energy absorbed by a layer during one time step
F_{ij} = interaction force between atoms i and j
$g(r)$ = radial distribution function
k_B = Boltzmann's constant
m = atomic mass
n = number density of atoms within a particle
N = number of atoms
r = position of the atom
r_c = cutoff distance
r_{ij} = the distance between atoms i and j
t = time
T = temperature
v = velocity of atoms
v' = velocity of atoms after scaling
$\overline{v}$ = average velocity of atoms

Greek Symbols

χ = scaling factor for the velocity of atoms
ε = LJ well depth parameter
ϕ = Lennard-Jones potential
σ_e = equilibrium separation parameter

τ = optical absorption depth

Subscripts

i = index of the atom
j = index of the atom/direction

References

[1] Kluge, M. D., Ray, J. R., and Rahman, A., 1987, ''Pulsed Laser Melting of Silicon: A Molecular Dynamics Study,'' J. Chem. Phys., **87**, pp. 2336–2339.

[2] Herrmann, R. F. W., Gerlach, J., and Campbell, E. E. B., 1998, ''Ultrashort Pulse Laser Ablation of Silicon: an MD Simulation Study,'' Appl. Phys. A: Mater. Sci. Process., **66**, pp. 35–42.

[3] Jeschke, H. O., Garcia, M. E., and Bennemann, K. H., 1999, ''Theory for Laser-induced Ultrafast Phase Transitions in Carbon,'' Appl. Phys. A: Mater. Sci. Process., **69**, pp. S49–S53.

[4] Häkkinen, H., and Landman, U., 1993, ''Superheating, Melting, and Annealing of Copper Surfaces,'' Phys. Rev. Lett., **71**, pp. 1023–1026.

[5] Anisimov, S. I., Kapeliovich, B. L., and Perelman, T. L., 1974, ''Electron Emission from Metal Surfaces Exposed to Ultra-short Laser Pulses,'' Sov. Phys. JETP, **39**, pp. 375–377.

[6] Ohmura, E., and Fukumoto, I., 1996, ''Molecular Dynamics Simulation on Laser Ablation of fcc Metal,'' Int. J. Jpn. Soc. Precis. Eng., **30**, pp. 128–133.

[7] Kotake, S., and Kuroki, M., 1993, ''Molecular Dynamics Study of Solid Melting and Vaporization by Laser Irradiation,'' Int. J. Heat Mass Transfer, **36**, pp. 2061–2067.

[8] Zhigilei, L. V., Kodali, P. B. S., and Garrison, B. J., 1997, ''Molecular Dynamics Model for Laser Ablation and Desorption of Organic Solids,'' J. Phys. Chem., **101**, pp. 2028–2037.

[9] Shibahara, M., and Kotake, S., 1998, ''Quantum Molecular Dynamics Study of Light-to-heat Absorption Mechanism in Atomic Systems,'' Int. J. Heat Mass Transfer, **41**, pp. 839–849.

[10] Silvestrelli, P. L., and Parrinello, M., 1998, ''Ab Initio Molecular Dynamics Simulation of Laser Melting of Graphite,'' J. Appl. Phys., **83**, pp. 2478–2483.

[11] Etcheverry, J. I., and Mesaros, M., 1999, ''Molecular Dynamics Simulation of the Production of Acoustic Waves by Pulsed Laser Irradiation,'' Phys. Rev. B, **60**, pp. 9430–9434.

[12] Wang, X., and Xu, X., 2002, ''Molecular Dynamics Simulation of Heat Transfer and Phase Change during Laser Material Interaction,'' ASME Journal of Heat Transfer, **124**, pp. 265–274.

[13] Wang, X., and Xu, X., 2003, ''Molecular Dynamics Simulation of Thermal and Thermomechanical Phenomena in Picosecond Laser Material Interaction,'' Int. J. Heat Mass Transfer, **46**, pp. 45–53.

[14] Zhigilei, L. V., and Garrison, B. J., 1999, ''Molecular Dynamics Simulation Study of the Fluence Dependence of Particle Yield and Plume Composition in Laser Desorption and Ablation of Organic Solids,'' Appl. Phys. Lett., **74**, pp. 1341–1343.

[15] Zhigilei, L. V., Kodali, P. B. S., and Garrison, B. J., 1998, ''A Microscopic View of Laser Ablation,'' J. Phys. Chem. B, **102**, pp. 2845–2853.

[16] Ohmura, E., Fukumoto, I., and Miyamoto, I., 1999, ''Modified Molecular Dynamics Simulation on Ultrafast Laser Ablation of Metal,'' *Proceedings of the International Congress on Applications of Lasers and Electro-Optics*, pp. 219–228.

[17] Allen, M. P., and Tildesley, D. J., 1987, *Computer Simulation of Liquids*, Clarendon Press, Oxford.

[18] Wang, X., and Xu, X., 2002, ''The Formation Process of Nanoparticles in Laser Materials Interaction,'' *2002 ASME International Mechanical Engineering Congress & Exposition*, Paper No. 33857, ASME, New York.